crystals

MDPI

Article

# Single Crystal Growth of Multiferroic Double Perovskites: $Yb_2CoMnO_6$ and $Lu_2CoMnO_6$

**Hwan Young Choi, Jae Young Moon, Jong Hyuk Kim, Young Jai Choi * and Nara Lee ***

Department of Physics and IPAP, Yonsei University, Seoul 120-749, Korea; lovesunice@gmail.com (H.Y.C.); jaissyy@naver.com (J.Y.M.); whsur1@gmail.com (J.H.K.)

* Correspondence: phylove@yonsei.ac.kr (Y.J.C.); eland@yonsei.ac.kr (N.L.); Tel.: +82-2-2123-5613 (Y.J.C. & N.L.)

Academic Editor: Iwan Kityk

Received: 29 January 2017; Accepted: 24 February 2017; Published: 27 February 2017

**Abstract:** We report on the growth of multiferroic $Yb_2CoMnO_6$ and $Lu_2CoMnO_6$ single crystals which were synthesized by the flux method with $Bi_2O_3$. $Yb_2CoMnO_6$ and $Lu_2CoMnO_6$ crystallize in a double-perovskite structure with a monoclinic $P2_1/n$ space group. Bulk magnetization measurements of both specimens revealed strong magnetic anisotropy and metamagnetic transitions. We observed a dielectric anomaly perpendicular to the $c$ axis. The strongly coupled magnetic and dielectric states resulted in the variation of both the dielectric constant and the magnetization by applying magnetic fields, offering an efficient approach to accomplish intrinsically coupled functionality in multiferroics.

**Keywords:** double perovskite; multiferroic; single crystal growth; flux method

## 1. Introduction

A multiferroic is a material that simultaneously exhibits ferroelectricity and magnetism [1–4]. Strong interplay between the electric and magnetic order parameters in multiferroics provides opportunities for novel device applications, such as magnetoelectric data storage and sensors [5–10]. In particular, in type-II multiferroics, ferroelectricity originates from the lattice relaxation via exchange strictions in a particular spin order with broken spatial inversion symmetry, which naturally leads to strong controllability of the dielectric properties via external magnetic fields [11–13].

Recently, a new type-II multiferroic was discovered: a double-perovskite structure of $Lu_2CoMnO_6$ [14–17]. From the polycrystalline work, the ferroelectricity was predicted to be along the crystallographic $c$ axis originating from the symmetric exchange striction of the up-up-down-down ($\uparrow\uparrow\downarrow\downarrow$) spin arrangement with alternating charge valences [15,17,18]. However, previous studies on single crystals revealed ferroelectricity perpendicular to the $c$ axis, which can be explained by the net polarization induced by the uniform oxygen displacements perpendicular to the $c$ axis on neighboring $\uparrow\uparrow\downarrow\downarrow$ spin chains when the symmetric exchange striction is activated [16–18]. $Lu_2CoMnO_6$ belongs to the double-perovskite $RE_2CoMnO_6$ series (RE = La, . . . , Lu). These materials crystallize in a monoclinic perovskite structure (space group $P2_1/n$) with alternating $Co^{2+}$ and $Mn^{4+}$ ions in a corner-shared oxygen octahedra [19]. In these compounds, additional antiferromagnetic clusters can arise from another valence state of $Co^{3+}$-$Mn^{3+}$ and antisites of ionic disorders and/or antiphase boundaries leading to $Co^{2+}$-$Co^{2+}$ or $Mn^{4+}$-$Mn^{4+}$ pairs [20]. As the size of rare earth ions decreases, the magnetic transition temperature decreases from 204 K for $La_2CoMnO_6$ [21] to 48 K for $Lu_2CoMnO_6$ [22].

We successfully grew single crystals of multiferroic $Yb_2CoMnO_6$ and $Lu_2CoMnO_6$ using the flux method with $Bi_2O_3$ flux. X-ray diffraction (XRD) confirmed the double-perovskite structure with a monoclinic $P2_1/n$ space group. The up-up-down-down ($\uparrow\uparrow\downarrow\downarrow$) spin order arose below $T_c$ = 52 and 48 K, respectively, leading to a dielectric anomaly perpendicular to the $c$ axis because of cooperative displacements of oxygen ions.

## 2. Experimental Methods

We synthesized single crystals of $Yb_2CoMnO_6$ (YCMO) and $Lu_2CoMnO_6$ (LCMO) by utilizing a conventional flux method with $Bi_2O_3$ flux in air [22]. Before the growth, the polycrystalline specimens were prepared by the solid-state reaction method. High purity powders of $Yb_2O_3$ ($Lu_2O_3$), $MnO_2$ and $Co_3O_4$ were mixed and ground in a mortar, followed by calcining at 1000 °C for 12 h in a box furnace. The calcined compound was finely re-ground and sintered at 1100 °C for 24 h. The same sintering procedure after regrinding was done at 1200 °C for 48 h. A mixture of pre-sintered YCMO (LCMO) polycrystalline powder and $Bi_2O_3$ flux with a ratio of 1:12 ratio was heated to 1300 °C in a Pt crucible, cooled slowly to 985 °C, and then cooled in a furnace after the power was turned off. The grown single crystals are shown in Figure 1.

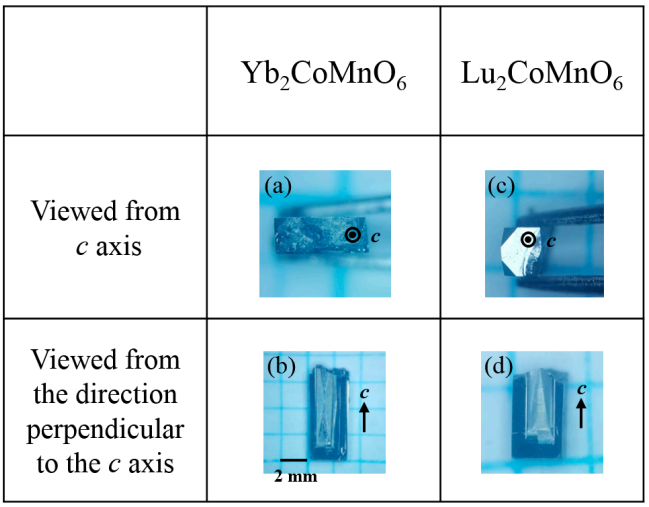


**Figure 1.** Images of representative single crystals of $Yb_2CoMnO_6$ (YCMO) (**a**,**b**) and $Lu_2CoMnO_6$ (LCMO) (**c**,**d**) viewed from the *c* axis and from the direction perpendicular to the *c* axis. The length of each side for the squares of grid pattern is 2 mm.

The crystallographic structures of both crystals were confirmed by a powder X-ray diffractometer (Ultima IV, Rigaku, Tokyo, Japan) using Cu-K radiation at room temperature. The detailed characterization for the structures was performed by Rietveld refinement by applying the FullProf software to the measured data. The temperature and magnetic-field dependence of magnetization for the single crystals were measured at temperatures of $T$ = 2–300 K under applied magnetic fields up to 9 T along ($H//c$) and perpendicular ($H\perp c$) to the *c* axis using a VSM technique in a Physical Properties Measurement System (PPMS, Quantum Design, San Diego, CA, USA). The temperature and magnetic-field dependence of the dielectric constant and the tangential loss under various magnetic fields were measured using a LCR meter (E4980, Agilent, Santa Clara, CA, USA).

## 3. Results

Figure 2 shows the XRD pattern for ground single crystals of YCMO and LCMO. Resulting from the Rietveld refinement [23], the crystal structure of YCMO (LCMO) was refined as a monoclinic double-perovskite structure ($P2_1/n$ space group) with good agreement factors, $\chi^2$ = 3.18 (4.89), $R_p$ = 7.78 (9.04)%, $R_{wp}$ = 6.62 (8.23)%, and $R_{exp}$ = 3.71 (3.72)%. Figure 3 shows the crystallographic structure of YCMO viewed from the *c* and *a* axes, respectively. $Co^{2+}$ and $Mn^{4+}$ ions were alternately located in corner-shared octahedral environments.

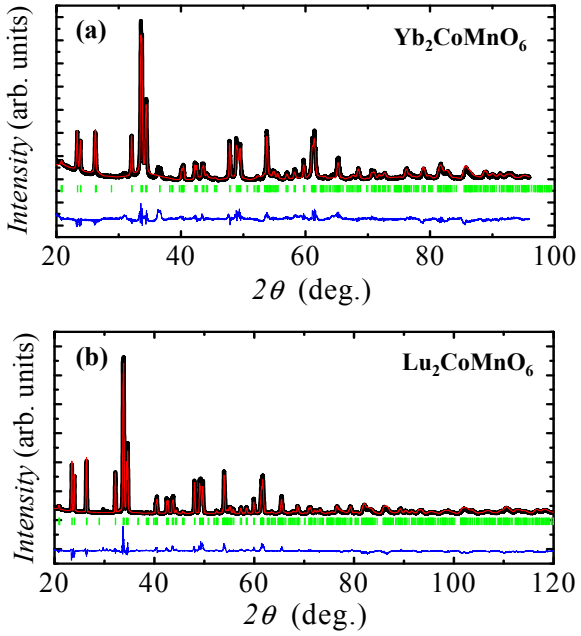


**Figure 2.** Observed (open circles) and calculated (solid line) powder XRD patterns for YCMO (**a**) and LCMO (**b**). The single phase of the monoclinic perovskite structure (space group $P2_1/n$) was identified.

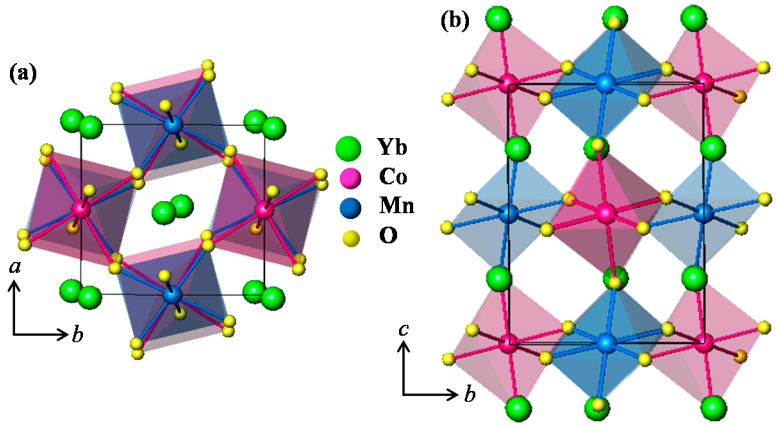


**Figure 3.** Views of the crystallographic structure of YCMO from the *c* axis (**a**) and the *a* axis (**b**). Green, red, blue and yellow spheres represent $Yb^{3+}$, $Co^{2+}$, $Mn^{4+}$, and $O^{2-}$ ions, respectively. The black box with the cross-section rectangles designates the crystallographic unit cell.

More specific refinement results are summarized in Tables 1 and 2, including the unit cell parameters, positional parameters, reliability factors, and bond lengths. $La_2CoMnO_6$ exhibited an almost pseudocubic structure with $a$ = 5.495 Å, $b$ = 5.492 Å, and $c/\sqrt{2}$ = 5.506 Å [22]. However, as the size of the rare earth ion decreases, the lattice constants $a$ and $c/\sqrt{2}$ also decrease linearly while $b$ slightly increases, which promotes the monoclinic distortion. The lattice constants for YCMO (LCMO), where the largest monoclinic distortion was developed, were $a$ = 5.194 (5.176) Å, $b$ = 5.568 (5.563) Å, and $c$ = 7.440 (7.434) Å with $\beta$ = 90.400 (90.431)°.

**Table 1.** Unit cell parameters, positional parameters, and reliability factors for YCMO and LCMO.

| | $Yb_2CoMnO_6$ | $Lu_2CoMnO_6$ |
|---|---|---|
| Structure | Monoclinic | Monoclinic |
| Space group | $P2_1/n$ | $P2_1/n$ |
| a (Å) | 5.19438 (6) | 5.17567 (9) |
| b (Å) | 5.56824 (7) | 5.56266 (9) |
| c (Å) | 7.44012 (9) | 7.43049 (13) |
| β (deg.) | 90.39966 (40) | 90.43100 (45) |
| V ($Å^3$) | 215.1895 | 213.9214 |
| Yb/ Lu (x, y, z) | 0.51951 (1)<br>0.54826 (5)<br>0.25018 (2) | 0.51905 (3)<br>0.57526 (1)<br>0.25111 (3) |
| Co (x, y, z) | (0.5, 0, 0) | (0.5, 0, 0) |
| Mn (x, y, z) | (0, 0.5, 0) | (0, 0.5, 0) |
| $O_1$ (x, y, z) | 0.38995 (7)<br>0.95622 (6)<br>0.26595 (11) | 0.37392 (18)<br>0.95756 (11)<br>0.26913 (16) |
| $O_2$ (x, y, z) | 0.15383 (12)<br>0.18749 (12)<br>−0.05387 (7) | 0.16546 (17)<br>0.19740 (16)<br>−0.06343 (10) |
| $O_3$ (x, y, z) | 0.28909 (16)<br>0.69364 (12)<br>−0.06026 (7) | 0.29886 (26)<br>0.67911 (24)<br>−0.051403 (16) |
| $R_p$ (%) | 7.78 | 9.04 |
| $R_{wp}$ (%) | 6.62 | 8.23 |
| $R_{exp}$ (%) | 3.71 | 3.72 |
| $\chi^2$ | 3.18 | 4.89 |

**Table 2.** Bond lengths for YCMO and LCMO.

| **Bond Length (Å)** | $Yb_2CoMnO_6$ | $Lu_2CoMnO_6$ |
|---|---|---|
| Yb/Lu-$O_1$ | 2.228 (4) | 2.141 (10) |
| Yb/Lu-$O_2$ | 2.167 (7) | 2.181 (9) |
| Yb/Lu-$O_3$ | 2.268 (7) | 2.26 (13) |
| Co-$O_1$ | 2.077 (8) | 2.121 (12) |
| Co-$O_2$ | 2.115 (7) | 2.101 (9) |
| Co-$O_3$ | 2.075 (8) | 2.100 (13) |
| Mn-$O_1$ | 1.845 (15) | 1.846 (12) |
| Mn-$O_2$ | 1.957 (7) | 1.948 (9) |
| Mn-$O_3$ | 1.905 (8) | 1.882 (15) |

Figure 4a,b show the temperature dependence of the anisotropic magnetic susceptibility for YCMO and LCMO, respectively, measured upon warming in $H$ = 0.01 T after zero-field cooling (ZFC) and upon cooling in the same $H$ (FC) for $H//c$ and $H\perp c$. The $\chi$ values for YCMO and LCMO exhibited pronounced peaks at $T_c$ = 52 and 48 K, respectively, which may correspond to a reentrant spin-glass behavior [24,25]. The temperature at which the ZFC and FC curves start to separate depends on the crystallographic orientations. The $\chi$ values for two different orientations exhibited strong magnetic anisotropy, which indicates that the spins were mainly aligned along the $c$ axis. A recent neutron diffraction study on polycrystalline LCMO suggested the up-up-down-down (↑↑↓↓) spin arrangement

along the *c* axis as the mostly probable magnetic ground state, originating from the frustrated exchange couplings [15,26].

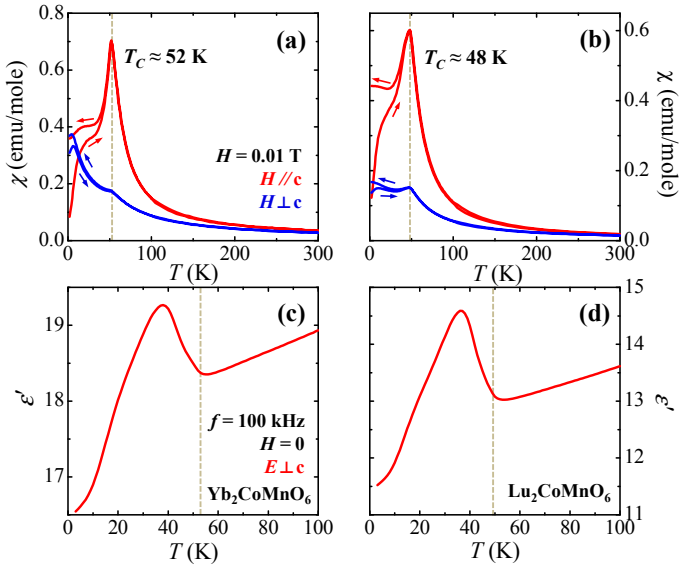


**Figure 4.** Temperature dependence of magnetic susceptibility, $\chi = M/H$ (1 emu = $4\pi \times 10^{-6}$ m$^3$), for YCMO (**a**) and LCMO (**b**) single crystals along ($H//c$) and perpendicular ($H \perp c$) to the *c* axis upon warming in $H = 0.01$ T after zero-magnetic-field cooling (ZFC) and upon cooling in the same field (FC). Temperature dependence of dielectric constant ($\varepsilon'$) perpendicular to the *c* axis in 0 T for YCMO (**c**) and LCMO (**d**) single crystals.

Figure 4c,d display the temperature dependence of the dielectric constant for YCMO and LCMO, respectively, measured perpendicular to the *c* axis in a zero-magnetic field. In both cases, the dielectric anomaly started from $T_c$, indicating a type-II multiferroic [7,14]. The broad peak in $H = 0$ T was observed below $T_c$ with a dielectric loss of less than 0.025, which is rationally small. The variation of the dielectric constant, which is defined as the peak height normalized by the value at $T_c$, can be estimated as ~5% and 12% for YCMO and LCMO, respectively. On the other hand, the estimated variation has been reported as small as ~3% and 2% in polycrystalline YCMO and LCMO, respectively. This difference reflects the fairly porous characteristic of polycrystalline structures [27,28].

The anisotropic isothermal magnetization at 2 K for $H//c$ and $H \perp c$ was measured after ZFC up to 9 T, as shown in Figure 5. In YCMO, the magnetization at 9 T in $H//c$ was ~7 $\mu_B$ per formula unit and was not saturated owing to the magnetic moments of $Yb^{3+}$ ions in addition to the magnetization of 6 $\mu_B$ for the $Co^{2+}$ ($S = 3/2$) and $Mn^{4+}$ ($S = 3/2$) moments in a formula unit [27]. It showed a large magnetic hysteresis with abrupt jumps at $\pm 1.4$ and 4.1 T. In LCMO, the initial curve of magnetization exhibited a metamagnetic spin-state transition from $\uparrow\uparrow\downarrow\downarrow$ to $\uparrow\uparrow\uparrow\uparrow$ at 2 T [29]. As the magnetic field decreased from 9 T, the magnetization showed consecutive metamagnetic transitions at 0.3, $-1.3$ and $-2.9$ T, which implies evolution from the saturation to several spin states, $\uparrow\uparrow\downarrow\downarrow$, $\uparrow\downarrow\downarrow\downarrow$, and $\downarrow\downarrow\downarrow\downarrow$ [30], similar to the Ising spin chain magnet of $Ca_3CoMnO_6$ [31].

Figure 6a,b display the derivative of isothermal magnetization, d$M$/d$H$, at 2 K and the field dependence of the dielectric constant at 2 K for YCMO. The dielectric constant exhibited sharp peaks at $\pm 1.4$ T and step-like features at $\pm 4.1$ T, consistent with the metamagnetic transitions shown as peaks of d$M$/d$H$. This simultaneous tunability demonstrated the manipulation of multiple order parameters in a type-II multiferroic. Figure 6c,d show the temperature dependence of the dielectric constants and the dielectric tangential losses, measured perpendicular to the *c* axis under various magnetic fields ($H = 0$, 1, 1.2, 1.4, 1.6, 1.8, 2 and 3 T) along the *c* axis for LCMO. Currently, the plausible explanation for the ferroelectricity can be given by the cooperative oxygen displacements perpendicular to the *c*

axis on neighboring ↑↑↓↓ spin chains because of the symmetric exchange strictions [31]. In LCMO, upon increasing the magnetic fields along the *c* axis, the broad peak was gradually suppressed and completely disappeared at 3 T where the magnetization was saturated. The dielectric loss exhibited a shoulder around the peak position of the dielectric constant and another peak below 20 K. The most distinct change occurred between 1.4 and 2 T, in accordance with the precipitous increase in the isothermal magnetization, indicating the strong interconnection between the dielectric and magnetic properties. The reduction of the peak in the dielectric constant can be explained by the metamagnetic spin-state transition from ↑↑↓↓ to ↑↑↑↑ as the fully saturated magnetic moments resulted in the cancelation of oxygen-ion shifts [14].

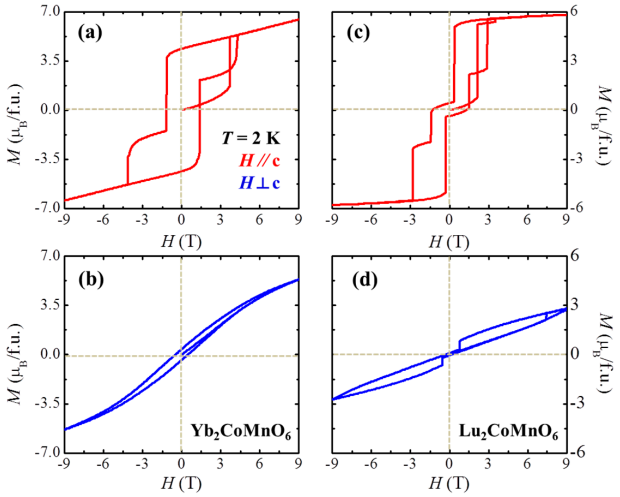


**Figure 5.** Isothermal magnetization along and perpendicular to the *c* axis measured at 2 K after ZFC for YCMO (**a**,**b**) and LCMO (**c**,**d**).

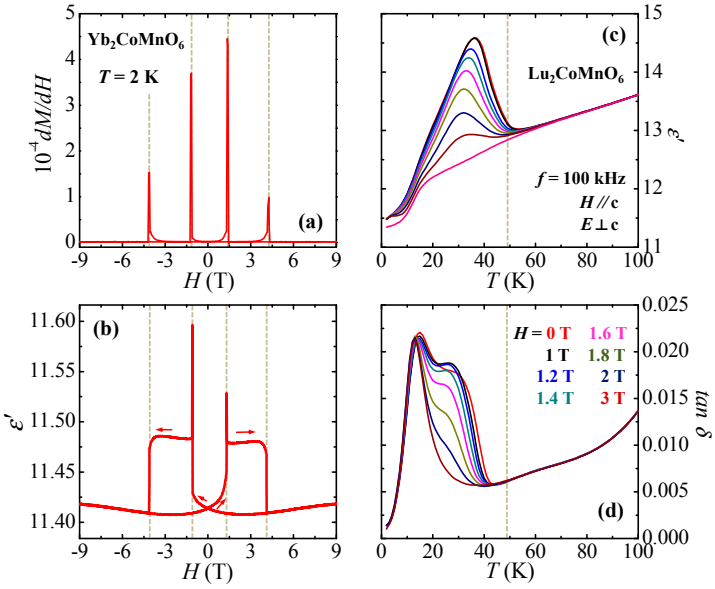


**Figure 6.** Derivative of isothermal magnetization at 2 K (**a**) and field dependence of dielectric constant ($\varepsilon'$) at 2 K (**b**) for YCMO. Temperature dependence of dielectric constant ($\varepsilon'$) and tangential loss (*tan δ*) perpendicular to the *c* axis under various magnetic fields (*H* = 0, 1, 1.2, 1.4, 1.6, 1.8, 2 and 3 T) along the *c* axis for LCMO (**c**,**d**).

## 4. Summary

The flux method was employed for the single-crystal growth of multiferroic $Yb_2CoMnO_6$ and $Lu_2CoMnO_6$ which crystallize in a double-perovskite structure with the monoclinic $P2_1/n$ space group. The refinement of the XRD data determines the lattice constants with large octahedral distortion as $a$ = 5.194 (5.176) Å, $b$ = 5.568 (5.563) Å, and $c$ = 7.440 (7.434) Å with $\beta$ = 90.400 (90.431)° for $Yb_2CoMnO_6$ ($Lu_2CoMnO_6$). The temperature and magnetic field dependences of the magnetization for both specimens exhibited a highly anisotropic nature and metamagnetic transitions. The simultaneous emergence of magnetic order and the dielectric anomaly indicates that both compounds are type-II multiferroics.

**Acknowledgments:** This work was supported by the NRF Grant (NRF-2014S1A2A2028481, NRF-2015R1C1A1A02037744, and NRF-2016R1C1B2013709) and partially by the Yonsei University Future-leading Research Initiative of 2014 (2015-22-0132).

**Author Contributions:** Hwan Young Choi, Jae Young Moon and Jong Hyuk Kim built the crystal growth apparatus and synthesized the crystals. Hwan Young Choi characterized the crystallogrphic structures. Hwan Young Choi and Jae Young Moon performed magnetic and dielectric measurements. Young Jai Choi and Nara Lee conceived of the project and managed the measurements. Hwan Young Choi, Young Jai Choi and Nara Lee analyzed the data and wrote the manuscript.

**Conflicts of Interest:** The authors declare no conflict of interest.

## References

1. Cheong, S.-W.; Mostovoy, M. Multiferroics: A magnetic twist for ferroelectricity. *Nat. Mater.* **2007**, *6*, 13–20. [CrossRef] [PubMed]
2. Eerenstein, W.; Mathur, N.D.; Scott, J.F. Multiferroic and magnetoelectric materials. *Nature* **2006**, *442*, 759–765. [CrossRef] [PubMed]
3. Wang, K.F.; Liu, J.M.; Ren, Z.F. Multiferroicity: The coupling between magnetic and polarization orders. *Adv. Phys.* **2009**, *58*, 321–448. [CrossRef]
4. Fiebig, M.; Lottermoser, T.; Meier, D.; Trassin, M. The evolution of multiferroics. *Nat. Rev. Mater.* **2016**, *1*, 16046. [CrossRef]
5. Hur, N.; Park, S.; Sharma, P.A.; Ahn, J.S.; Guha, S.; Cheong, S.W. Electric polarization reversal and memory in a multiferroic material induced by magnetic fields. *Nature* **2004**, *429*, 392–395. [CrossRef] [PubMed]
6. Wu, S.M.; Cybart, S.A.; Yu, P.; Rossell, M.D.; Zhang, J.X.; Ramesh, R.; Dynes, R.C. Reversible electric control of exchange bias in a multiferroic field-effect device. *Nat. Mater.* **2010**, *9*, 756–761. [CrossRef] [PubMed]
7. Kimura, T.; Goto, T.; Shintani, H.; Ishizaka, K.; Arima, T.; Tokura, Y. Magnetic control of ferroelectric polarization. *Nature* **2003**, *426*, 55–58. [CrossRef] [PubMed]
8. Spaldin, N.A.; Fiebig, M. The renaissance of magnetoelectric multiferroics. *Science* **2005**, *309*, 391–392. [CrossRef] [PubMed]
9. Kitagawa, Y.; Hiraoka, Y.; Honda, T.; Ishikura, T.; Nakamura, H.; Kimura, T. Low-field magnetoelectric effect at room temperature. *Nat. Mater.* **2010**, *9*, 797–802. [CrossRef] [PubMed]
10. Seki, S.; Yu, X.Z.; Ishiwata, S.; Tokura, Y. Observation of skyrmions in a multiferroic material. *Science* **2012**, *336*, 198–201. [CrossRef] [PubMed]
11. Lee, N.; Vecchini, C.; Choi, Y.J.; Chapon, L.C.; Bombardi, A.; Radaelli, P.G.; Cheong, S.W. Giant tunability of ferroelectric polarization in $GdMn_2O_5$. *Phys. Rev. Lett.* **2013**, *110*, 137203. [CrossRef] [PubMed]
12. Su, J.; Yang, Z.Z.; Lu, X.M.; Zhang, J.T.; Gu, L.; Lu, C.J.; Li, Q.C.; Liu, J.M.; Zhu, J.S. Magnetism-Driven Ferroelectricity in Double Perovskite $Y_2NiMnO_6$. *ACS Appl. Mater. Interfaces* **2015**, *7*, 13260–13265. [CrossRef] [PubMed]
13. Ishihara, S. Electronic ferroelectricity and frustration. *J. Phys. Soc. Jpn.* **2010**, *79*, 011010. [CrossRef]
14. Lee, N.; Choi, H.Y.; Jo, Y.J.; Seo, M.S.; Park, S.Y.; Choi, Y.J. Strong ferromagnetic-dielectric coupling in multiferroic $Lu_2CoMnO_6$ single crystals. *Appl. Phys. Lett.* **2014**, *104*, 112907. [CrossRef]
15. Yáñez-Vilar, S.; Mun, E.D.; Zapf, B.G.; Ueland, B.G.; Gardner, J.S.; Thompson, J.D.; Singleton, J.; Sánchez-Andújar, M.; Mira, J.; Biskup, N.; et al. Multiferroic behavior in the double-perovskite $Lu_2MnCoO_6$. *Phys. Rev. B* **2011**, *84*, 134427.

16. Chikara, S.; Singleton, J.; Bowlan, J.; Yarotski, D.A.; Lee, N.; Choi, H.Y.; Choi, Y.J.; Zapf, V.S. Electric polarization observed in single crystals of multiferroic $Lu_2MnCoO_6$. *Phys. Rev. B* **2016**, *93*, 180405. [CrossRef]
17. Zhang, J.T.; Lu, X.M.; Yang, X.Q.; Wang, J.L.; Zhu, J.S. Origins of ↑↑↓↓ magnetic structure and ferroelectricity in multiferroic $Lu_2CoMnO_6$. *Phys. Rev. B* **2016**, *93*, 075140. [CrossRef]
18. Zhou, H.Y.; Zhao, H.J.; Zhang, W.Q.; Chen, X.M. Magnetic domain wall induced ferroelectricity in double perovskites. *Appl. Phys. Lett.* **2015**, *106*, 152901. [CrossRef]
19. Vasiliev, A.N.; Volkova, O.S.; Lobanovskii, L.S.; Troyanchuk, I.O.; Hu, Z.; Tjeng, L.H.; Khomskii, D.I.; Lin, H.-J.; Chen, C.T.; Tristan, N. Valence states and metamagnetic phase transition in partially *B*-site-disordered perovskite $EuMn_{0.5}Co_{0.5}O_3$. *Phys. Rev. B* **2008**, *77*, 104442. [CrossRef]
20. Nair, H.S.; Pradheesh, R.; Xiao, Y.; Cherian, D.; Elizabeth, S.; Hansen, T.; Chatterji, T.; Brückel, T. Magnetization-steps in $Y_2CoMnO_6$ double perovskite: The role of antisite disorder. *J. Appl. Phys.* **2014**, *116*, 123907. [CrossRef]
21. Kim, M.K.; Moon, J.Y.; Choi, H.Y.; Oh, S.H.; Lee, N.; Choi, Y.J. Effects of different annealing atmospheres on magnetic properties in $La_2CoMnO_6$ single crystals. *Curr. Appl. Phys.* **2015**, *15*, 776. [CrossRef]
22. Kim, M.K.; Moon, J.Y.; Choi, H.Y.; Oh, S.H.; Lee, N.; Choi, Y.J. Investigation of the magnetic properties in double perovskite $R_2CoMnO_6$ single crystals (R = rare earth: La to Lu). *J. Phys. Condens. Matter* **2015**, *27*, 426002. [CrossRef] [PubMed]
23. Rodríguez-Carvajal, J. Recent advances in magnetic structure determination by neutron powder diffraction. *Phys. B Condens. Matter* **1993**, *192*, 55–59. [CrossRef]
24. Dho, J.; Kim, W.S.; Hur, N.H. Reentrant spin glass behavior in Cr-doped perovskite manganite. *Phys. Rev. Lett.* **2002**, *89*, 027202. [CrossRef] [PubMed]
25. Viswanathan, M.; Kumar, P.S.A. Observation of reentrant spin glass behavior in $LaCo_{0.5}Ni_{0.5}O_3$. *Phys. Rev. B* **2009**, *80*, 012410. [CrossRef]
26. Fisher, M.E.; Selke, W. Infinitely many commensurate phases in a simple Ising model. *Phys. Rev. Lett.* **1980**, *44*, 1502. [CrossRef]
27. Blasco, J.; García-Muñoz, J.L.; García, J.; Stankiewicz, J.; Subías, G.; Ritter, C.; Rodríguez-Velamazán, J.A. Evidence of large magneto-dielectric effect coupled to a metamagnetic transition in $Yb_2CoMnO_6$. *Appl. Phys. Lett.* **2015**, *107*, 012902. [CrossRef]
28. Cui, Y.; Zhang, L.; Xie, G.; Wang, R. Magnetic and transport and dielectric properties of polycrystalline $TbMnO_3$. *Solid State Commun.* **2006**, *138*, 481. [CrossRef]
29. Dho, J.; Hur, N.H. Thermal relaxation of field-induced irreversible ferromagnetic phase in Pr-doped manganites. *Phys. Rev. B* **2003**, *67*, 214414. [CrossRef]
30. Xin, C.; Sui, Y.; Wang, Y.; Wang, Y.; Wang, X.; Liu, Z.; Li, B.; Liu, X. Spin rotation driven ferroelectric polarization with a 180° flop in double-perovskite $Lu_2CoMnO_6$. *RSC Adv.* **2015**, *5*, 43432–43439. [CrossRef]
31. Choi, Y.J.; Yi, H.T.; Lee, S.; Huang, Q.; Kiryukhin, V.; Cheong, S.W. Ferroelectricity in an Ising chain magnet. *Phys. Rev. Lett.* **2008**, *100*, 047601. [CrossRef] [PubMed]